

# Fitting the Constitution SNIa Data with Redshift Binned Parameterization Method

Qing-Guo Huang,<sup>1,2,\*</sup> Miao Li,<sup>2,3,†</sup> Xiao-Dong Li,<sup>4,3,‡</sup> and Shuang Wang<sup>5,3,§</sup>

<sup>1</sup>*School of Physics, Korea Institute of Advanced Study, Seoul 130722, Korea*

<sup>2</sup>*Kavli Institute for Theoretical Physics China,  
Chinese Academy of Sciences, Beijing 100190, China*

<sup>3</sup>*Key Laboratory of Frontiers in Theoretical Physics, Institute of Theoretical Physics,  
Chinese Academy of Sciences, Beijing 100190, China*

<sup>4</sup>*Interdisciplinary Center for Theoretical Study,  
University of Science and Technology of China, Hefei 230026, China*

<sup>5</sup>*Department of Modern Physics, University of Science and Technology of China, Hefei 230026, China*

In this work, we explore the cosmological consequences of the recently released Constitution sample of 397 Type Ia supernovae (SNIa). By revisiting the Chevallier-Polarski-Linder (CPL) parameterization, we find that, for fitting the Constitution set alone, the behavior of dark energy (DE) significantly deviate from the cosmological constant  $\Lambda$ , where the equation of state (EOS)  $w$  and the energy density  $\rho_\Lambda$  of DE will rapidly decrease along with the increase of redshift  $z$ . Inspired by this clue, we separate the redshifts into different bins, and discuss the models of a constant  $w$  or a constant  $\rho_\Lambda$  in each bin, respectively. It is found that for fitting the Constitution set alone,  $w$  and  $\rho_\Lambda$  will also rapidly decrease along with the increase of  $z$ , which is consistent with the result of CPL model. Moreover, a step function model in which  $\rho_\Lambda$  rapidly decreases at redshift  $z \sim 0.331$  presents a significant improvement ( $\Delta\chi^2 = -4.361$ ) over the CPL parameterization, and performs better than other DE models. We also plot the error bars of DE density of this model, and find that this model deviates from the cosmological constant  $\Lambda$  at 68.3% confidence level (CL); this may arise from some biasing systematic errors in the handling of SNIa data, or more interestingly from the nature of DE itself. In addition, for models with same number of redshift bins, a piecewise constant  $\rho_\Lambda$  model always performs better than a piecewise constant  $w$  model; this shows the advantage of using  $\rho_\Lambda$ , instead of  $w$ , to probe the variation of DE.

---

\*Electronic address: huangqg@kias.re.kr

†Electronic address: mli@itp.ac.cn

‡Electronic address: renzhe@mail.ustc.edu.cn

§Electronic address: swang@mail.ustc.edu.cn

## I. INTRODUCTION

Although it has been a decade since the discovery of the cosmic acceleration [1, 2], the nature of dark energy (DE) still remains a mystery. The most obvious theoretical candidate of DE is the cosmological constant  $\Lambda$ , which can fit observations well, but is plagued with the fine-tuning problem and the coincidence problem [3]. Numerous other dynamical DE models have also been proposed in the literature, such as quintessence [4], phantom [5],  $k$ -essence [6], tachyon [7], holographic [8], agegraphic [9], hessence [10], Chaplygin gas [11], Yang-Mills condensate [12], ect.

A most powerful probe of DE is Type Ia supernovae (SNIa), which can be used as cosmological standard candles to measure directly the expansion history of the universe. A large sample of nearby SNIa with  $z < 0.08$  has recently been published [13]. Adding this to the Union sample [14] leads to the so-called Constitution set [15] which is currently the largest SNIa sample to date. By analyzing this Constitution set with Chevallier-Polarski-Linder (CPL) ansatz [16], Shafieloo et al. [17] argue that cosmic acceleration may have already peaked and that we are currently witnessing its slowing down. By separating the redshifts into different bins and assuming a constant equation of state (EOS)  $w$  in each bin, Qi et al. [18] also point out that this Constitution set shows a deviation at 68.3% confidence level (CL) from the  $\Lambda$ CDM model. Besides, by studying the constraints of DE on the  $w - w'$  plane, Chen et al. [19] claim that  $\Lambda$ CDM model is disfavored by the current observational data at 68.3% confidence.

Although constraining EOS  $w$  of DE is a popular and widely-used method to investigate dark energy, Wang and Freese [20] pointed out that DE density  $\rho_\Lambda$  can be constrained more tightly than EOS  $w$  given the same observational data. Therefore, it would also be very interesting to consider the cases of piecewise constant  $\rho_\Lambda$ . In this work we separate the redshifts into different bins, and discuss the models of a constant  $w$  or a constant  $\rho_\Lambda$  in each bin, respectively. Binned fits of EOS have been applied before in [21] [22] [23], and the Union paper itself [14]. Similar analyses have been performed for density binning [20]. Our paper differs from previous ones in two aspects: First, in previous papers the redshift bins are determined by setting the discontinuity points of redshift by hand, while in our paper we treat the discontinuity points of redshift as free parameters, and find that much smaller  $\chi_{min}^2$  can be obtained. Second, not only the piecewise constant  $w$  models but also the piecewise constant  $\rho_\Lambda$  models are considered in this work. Moreover, by comparing these two classes of model, it is found that for same number of redshift bins, a piecewise constant  $\rho_\Lambda$  model always performs better than a piecewise constant  $w$  model.

This work is organized as follows. In Section 2, we briefly review the models considered here and the method of data analysis. In Section 3, we introduce the observational data and describe how they are included in our analysis. Section 4 is divided into three parts: First of all, we revisit the CPL model and

find that for fitting the Constitution set alone the behavior of DE significantly deviate from the cosmological constant  $\Lambda$ , where  $w$  and  $\rho_\Lambda$  will rapidly decrease along with the increase of redshift  $z$ . This result implies that the behavior of dark energy might be very different in different slices of redshifts, and inspires us to separate redshifts into several bins and to investigate the piecewise constant  $w$  model and the piecewise constant  $\rho_\Lambda$  model. Then, we discuss the models with two bins. It is found that for fitting the Constitution set alone,  $\rho_\Lambda$  will also rapidly decrease along with the increase of  $z$ , which is consistent with the result of CPL model. Moreover, a step function model in which  $\rho_\Lambda$  rapidly decreases at redshift  $z \sim 0.331$  presents a significant improvement ( $\Delta\chi^2 = -4.361$ ) over the CPL parameterization, and performs better than other DE models. We also plot the error bars of  $\rho_\Lambda$  of this model, and find that this model deviates from the cosmological constant  $\Lambda$  at 68.3% confidence level. Next, we briefly discuss the models with three bins, and find that the cases of three bins are very similar with that of two bins. At last, we give a short summary in Section 5. In this work, we assume today's scale factor  $a_0 = 1$ , so the redshift  $z$  satisfies  $z = a^{-1} - 1$ ; the subscript "0" always indicates the present value of the corresponding quantity, and the unit with  $c = \hbar = 1$  is used.

## II. MODEL AND METHODOLOGY

Standard candles impose constraints on cosmological parameters essentially through a comparison of the luminosity distance from observation with that from theoretical models. In a spatially flat Friedmann-Robertson-Walker (FRW) universe (the assumption of flatness is motivated by the inflation scenario), the luminosity distance  $d_L$  is given by

$$d_L(z) = \frac{1+z}{H_0} \int_0^z \frac{dz'}{E(z')}, \quad (1)$$

with

$$E(z) \equiv H(z)/H_0 = \left[ \Omega_{m0}(1+z)^3 + (1 - \Omega_{m0})f(z) \right]^{1/2}, \quad (2)$$

where  $H(z)$  is the Hubble parameter,  $H_0$  is the Hubble constant,  $\Omega_{m0}$  is the present fractional matter density, and  $f(z) \equiv \rho_\Lambda(z)/\rho_{\Lambda 0}$  is a key function, because DE parameterization schemes enter through  $f(z)$ .

We will consider the familiar CPL ansatz [16], in which the EoS of DE is parameterized as

$$w = w_0 + w_1 \frac{z}{1+z}, \quad (3)$$

where  $w_0$  and  $w_1$  are constants. As is well known, the corresponding  $f(z)$  is given by

$$f(z) = (1+z)^{3(1+w_0+w_1)} \exp\left(-\frac{3w_1 z}{1+z}\right). \quad (4)$$

For the case where EOS  $w$  is piecewise constant in redshift,  $f(z)$  can be written as [22, 23]

$$f(z_{n-1} < z \leq z_n) = (1+z)^{3(1+w_n)} \prod_{i=0}^{n-1} (1+z_i)^{3(w_i-w_{i+1})}, \quad (5)$$

where  $w_i$  is the EOS parameter in the  $i^{\text{th}}$  redshift bin defined by an upper boundary at  $z_i$ . This class of models has been extensively studied in the literature. As mentioned above, it is interesting to consider the piecewise constant  $\rho_\Lambda$  models. For this case,  $f(z)$  can be written as

$$f(z) = \begin{cases} 1 & 0 \leq z \leq z_1 \\ \epsilon_n & z_{n-1} \leq z \leq z_n \quad (n > 1) \end{cases}. \quad (6)$$

Here  $\epsilon_n$  is a piecewise constant, and from the relation  $E(0) = 1$  one can easily obtain  $\epsilon_1 = 1$ . So for same number of redshift bins, the number of free parameters of piecewise constant  $\rho_\Lambda$  model is one fewer than that of piecewise constant  $w$  model. It should be mentioned that there are different opinions in the literature about the optimal choice of redshift bins in constraining DE. In [22, 23], the authors directly set the discontinuity points of redshift as  $z_1 = 0.2$ ,  $z_2 = 0.5$ , and  $z_3 = 1.8$ . In [24], Wang argue that one should choose a constant  $\Delta z$  for redshift slices. In this work, we just treat the discontinuity points of redshift as model parameters in performing the best-fit analysis. As seen below, this leads to a much smaller  $\chi_{min}^2$ .

In this work we adopt  $\chi^2$  statistic to estimate parameters. For a physical quantity  $\xi$  with experimentally measured value  $\xi_o$ , standard deviation  $\sigma_\xi$ , and theoretically predicted value  $\xi_t$ , the  $\chi^2$  value is given by

$$\chi_\xi^2 = \frac{(\xi_t - \xi_o)^2}{\sigma_\xi^2}. \quad (7)$$

The total  $\chi^2$  is the sum of all  $\chi_\xi^2$ s, i.e.

$$\chi^2 = \sum_{\xi} \chi_\xi^2. \quad (8)$$

Assuming the measurement errors be Gaussian, the likelihood function is given by

$$\mathcal{L} \propto e^{-\chi^2/2}. \quad (9)$$

For comparing different models, a statistical variable must be chosen. The  $\chi_{min}^2$  is the simplest one, but it has difficulty to compare different models with different number of parameters. In this work, we will use  $\chi_{min}^2/dof$  as a model selection criterion, where  $dof$  is the degree of freedom defined as

$$dof \equiv N - k, \quad (10)$$

here  $N$  is the number of data, and  $k$  is the number of free parameters. Besides, to compare different models with different number of parameters, people often use the Bayesian information criterion [25] given by [26]

$$BIC = -2 \ln \mathcal{L}_{max} + k \ln N, \quad (11)$$

where  $\mathcal{L}_{max}$  is the maximum likelihood. It is clear that a model favored by the observations should give smaller  $\chi^2_{min}/dof$  and  $BIC$ .

### III. OBSERVATIONAL DATA

#### A. Type Ia supernovae

For SNIa data, we use the latest 397 Constitution sample, the distance modulus  $\mu_{obs}(z_i)$ , compiled in Table 1 of [15]. The theoretical distance modulus is defined as

$$\mu_{th}(z_i) \equiv 5 \log_{10} D_L(z_i) + \mu_0, \quad (12)$$

where  $\mu_0 \equiv 42.38 - 5 \log_{10} h$  with  $h$  the Hubble constant  $H_0$  in units of 100 km/s/Mpc, and

$$D_L(z) = (1+z) \int_0^z \frac{dz'}{E(z'; \theta)} \quad (13)$$

is the Hubble-free luminosity distance  $H_0 d_L$  in a spatially flat FRW universe, and here  $\theta$  denotes the model parameters. The  $\chi^2$  for the SNIa data is

$$\chi_{SN}^2(\theta) = \sum_{i=1}^{397} \frac{[\mu_{obs}(z_i) - \mu_{th}(z_i)]^2}{\sigma_i^2}, \quad (14)$$

where  $\mu_{obs}(z_i)$  and  $\sigma_i$  are the observed value and the corresponding  $1\sigma$  error of distance modulus for each supernova, respectively. The parameter  $\mu_0$  is a nuisance parameter but it is independent of the data and the dataset. Following [27], the minimization with respect to  $\mu_0$  can be made trivial by expanding the  $\chi^2$  of Eq.(14) with respect to  $\mu_0$  as

$$\chi_{SN}^2(\theta) = A(\theta) - 2\mu_0 B(\theta) + \mu_0^2 C, \quad (15)$$

where

$$A(\theta) = \sum_{i=1}^{397} \frac{[\mu_{obs}(z_i) - \mu_{th}(z_i; \mu_0 = 0, \theta)]^2}{\sigma_i^2}, \quad (16)$$

$$B(\theta) = \sum_{i=1}^{397} \frac{\mu_{obs}(z_i) - \mu_{th}(z_i; \mu_0 = 0, \theta)}{\sigma_i^2}, \quad (17)$$

$$C = \sum_{i=1}^{397} \frac{1}{\sigma_i^2}. \quad (18)$$

Evidently, Eq. (14) has a minimum for  $\mu_0 = B/C$  at

$$\tilde{\chi}_{SN}^2(\theta) = A(\theta) - \frac{B(\theta)^2}{C}. \quad (19)$$

Since  $\chi_{SN,min}^2 = \tilde{\chi}_{SN,min}^2$ , instead minimizing  $\chi_{SN}^2$  one can minimize  $\tilde{\chi}_{SN}^2$  which is independent of the nuisance parameter  $\mu_0$ .

## B. Baryon Acoustic Oscillations

For BAO data, we consider the parameter  $A$  from the measurement of the BAO peak in the distribution of SDSS luminous red galaxies, which is defined as [28]

$$A \equiv \Omega_{m0}^{1/2} E(z_b)^{-1/3} \left[ \frac{1}{z_b} \int_0^{z_b} \frac{dz'}{E(z')} \right]^{2/3}, \quad (20)$$

where  $z_b = 0.35$ . The SDSS BAO measurement [28] gives  $A_{obs} = 0.469 (n_s/0.98)^{-0.35} \pm 0.017$ , where the scalar spectral index is taken to be  $n_s = 0.960$  as measured by WMAP5 [29]. It is widely believed that  $A$  is nearly model-independent and can provide robust constraint as complement to SNIa data. The  $\chi^2$  for the BAO data is

$$\chi_{BAO}^2 = \frac{(A - A_{obs})^2}{\sigma_A^2}, \quad (21)$$

where the corresponding  $1\sigma$  errors is  $\sigma_A = 0.017$ .

## C. cosmic microwave background

For CMB data, we use the CMB shift parameter  $R$ , which is given by [30, 31]

$$R \equiv \Omega_{m0}^{1/2} \int_0^{z_{rec}} \frac{dz'}{E(z')}, \quad (22)$$

where the redshift of recombination  $z_{rec} = 1090$  [29]. The shift parameter  $R$  relates the angular diameter distance to the last scattering surface, the comoving size of the sound horizon at  $z_{rec}$  and the angular scale of the first acoustic peak in CMB power spectrum of temperature fluctuations [30, 31]. The measured value of  $R$  has been updated to be  $R_{obs} = 1.710 \pm 0.019$  from WMAP5 [29]. It should be noted that, different from the SNIa and BAO data, the  $R$  parameter can provide the information about the universe at very high redshift. The  $\chi^2$  for the CMB data is

$$\chi_{CMB}^2 = \frac{(R - R_{obs})^2}{\sigma_R^2}, \quad (23)$$

where the corresponding  $1\sigma$  errors is  $\sigma_R = 0.019$ .

## IV. RESULTS

### A. CPL parameterization

We will present the results of CPL parameterization in this subsection. It is found that  $\chi_{min}^2 = 461.254$ , 465.440, and 466.100 for SNIa, SNIa+BAO, and SNIa+BAO+CMB data, respectively. Moreover, we

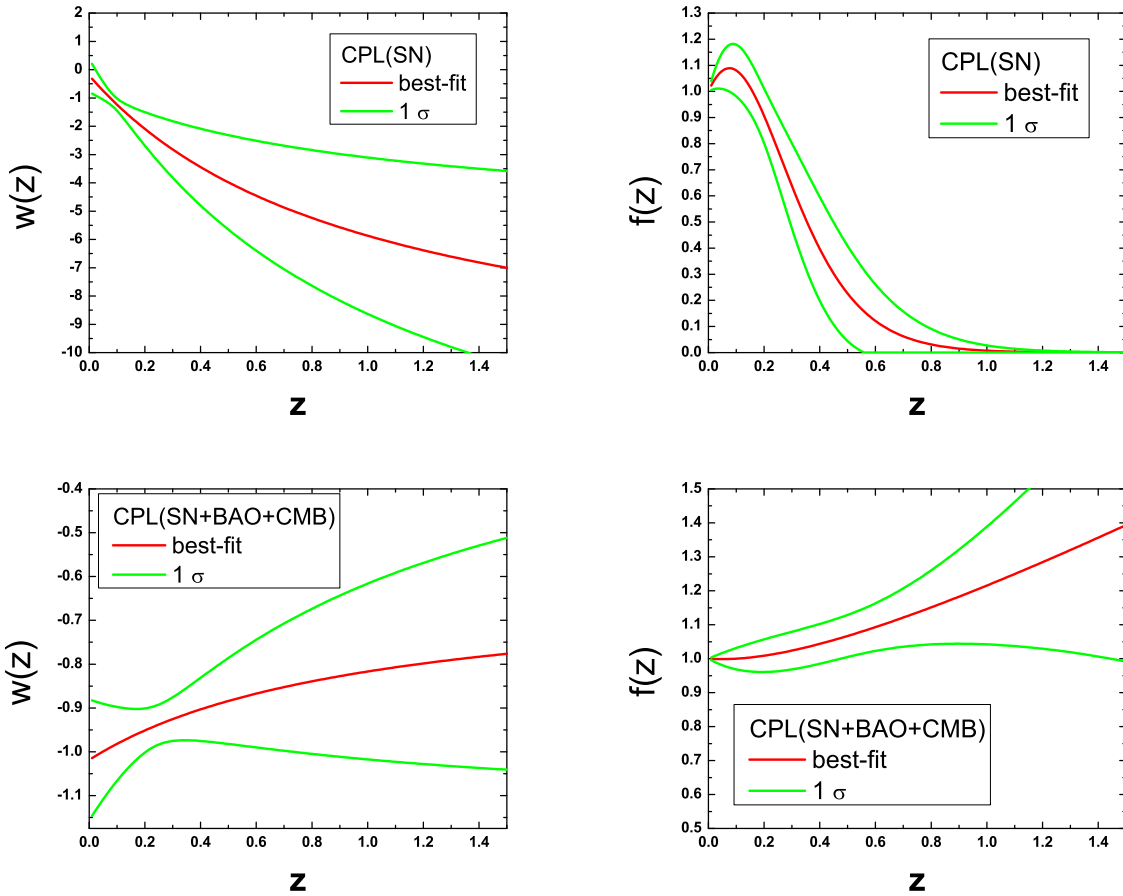


FIG. 1: Reconstructed  $w(z)$  and  $f(z)$  from SnIa data alone (upper panel) and SnIa+BAO+CMB data(lower panel) using the CPL ansatz. Red lines stand for the best-fit values and green lines stand for the  $1\sigma$  CL.

reconstruct  $w(z)$  and  $f(z)$  by using CPL parameterization, as is shown in figure 1. The upper panel of figure 1 shows reconstructed  $w(z)$  and  $f(z)$  from SnIa data alone. From this panel, it is seen that  $w$  and  $f$  (i.e. DE density  $\rho_\Lambda$ ) will rapidly decrease along with the increase of redshift  $z$ , and the behavior of DE significantly deviate from the cosmological constant  $\Lambda$  at  $1\sigma$  CL. It should be mentioned that our results are consistent with some other works. For example. Figure 2 of [17] shows that the best-fit value of  $w_1$  is rather negative. This means that the EOS  $w$  of DE will also be quite negative at high-redshift region.

The lower panel of figure 1 shows reconstructed  $w(z)$  and  $f(z)$  from SnIa+BAO+CMB data. For this case, the result is quite different, and the  $\Lambda$ CDM model is still consistent with observational data at  $1\sigma$  CL. The difference from these two panels of figure 1 shows the existence of the tension among different types of observational data, which was recently discussed in [32]. Their result of the CPL parametrization shows that for the Union compilation when CMB and BAO data is added there is a  $\Delta\chi^2 = 1.063$ , while for the Constitution set  $\Delta\chi^2 = 4.846$ , which is much larger. Their result is consistent with ours. Besides, in [33]

the authors get  $(w_0, w_1) = (-0.95_{-0.18}^{+0.45}, 0.41_{-0.96}^{+0.79})$  for the CPL parametrization from SNIa+BAO data, which shows the existence of tension between SNIa and BAO data compared with the upper pannel of figure 1.

As mention above, for fitting SNIa data alone, we find that both  $w$  and  $\rho_\Lambda$  will rapidly decrease along with the increase of redshift  $z$  by using CPL parameterization. This result implies that the behavior of dark energy might be very different in different slices of redshifts, and inspires us to separate redshifts into several bins and to investigate the piecewise constant  $w$  model and the piecewise constant  $\rho_\Lambda$  model.

## B. $\Lambda$ CDM2 and XCDM2 Model

Let us discuss the cases in which redshifts are separated into 2bins. Hereafter we will call 2 bins piecewise constant  $w$  model as XCDM2 model, and will call 2 bins piecewise constant  $\rho_\Lambda$  model as  $\Lambda$ CDM2 model.

Figure 2 shows the  $\chi_{min}^2$  versus redshift  $z$  for XCDM2 and  $\Lambda$ CDM2 models, where only the Constitution SNIa sample is used in the analysis. It is seen that the curves of  $\chi_{min}^2$  of these two models are very similar, and both these two models achieve their minimal  $\chi_{min}^2$  at the discontinuity points of redshift  $z_1 = 0.331$ . We will analyze the XCDM2 and  $\Lambda$ CDM2 model more explicitly at this discontinuity point. The result is as follows.

For XCDM2 model, using the SNIa data and the discontinuity point  $z_1 = 0.331$ , we find that the best-fit value and Corresponding  $1\sigma$  CL of the model parameters are  $\Omega_{m0} = 0.466_{-0.032}^{+0.037}$ ,  $w_0 = -1.118_{-0.418}^{+0.342}$ , and  $w_1$  with the best-fit value  $-508.170$  and the upper  $1\sigma$  CL value  $-15.2$ . For this model,  $\chi_{min}^2 = 456.574$  (As a comparison, for the CPL parametrization to the same data, the  $\chi_{min}^2 = 461.254$ . The XCDM2 model lower the  $\chi_{min}^2$  by 4.32). Notice that the EOS of the second redshift slice  $w_1 \ll -1$ , this means the DE density  $\rho_\Lambda$  should decay very quickly at the range  $z > 0.331$ .

For  $\Lambda$ CDM2 model, using the SNIa data and the discontinuity point  $z_1 = 0.331$ , we find that the best-fit value and Corresponding  $1\sigma$  CL of the model parameters are  $\Omega_{m0} = 0.461_{-0.092}^{+0.128}$  and  $\epsilon_2 = (5.407 \times 10^{-7})_{-0.462}^{+0.348}$ , corresponding to  $\chi_{min}^2 = 456.893$ . Notice that the best-fit  $\Omega_{m0}$  and the  $\chi_{min}^2$  is very close to the result of the XCDM2 model. We also plot the  $1\sigma$  and  $2\sigma$  error bars for the  $\Lambda$ CDM2 model in figure 3. It is seen that there is a deviation from cosmological constant  $\Lambda$  over  $1\sigma$  confidence level, which is similar to the results of CPL parameterization and XCDM2 model.

To further verify this conclusion, we construct three toy models to mimic the step function, as is listed in table I, and analyze them using the SNIa data. It is found that, for toy model 1, the best-fit model parameters are  $\Omega_{m0} = 0.457$  and  $\xi = 3.734 \times 10^{-11}$ , corresponding to  $\chi_{min}^2 = 457.805$ ; for toy model 2, the best-fit model



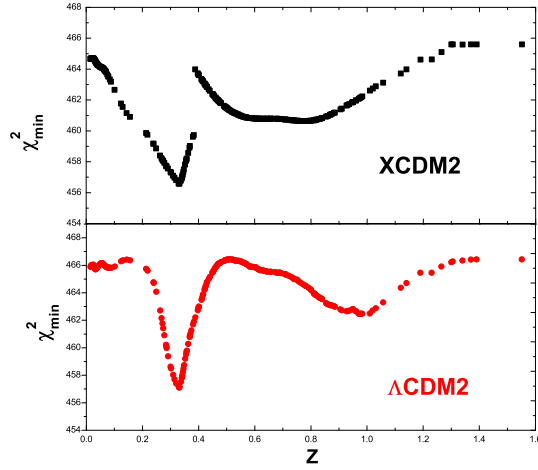


FIG. 2:  $\chi_{min}^2$  versus redshift  $z$  for XCDM2 model and for  $\Lambda$ CDM2 model. Only the Constitution SNIa sample is used in the analysis.

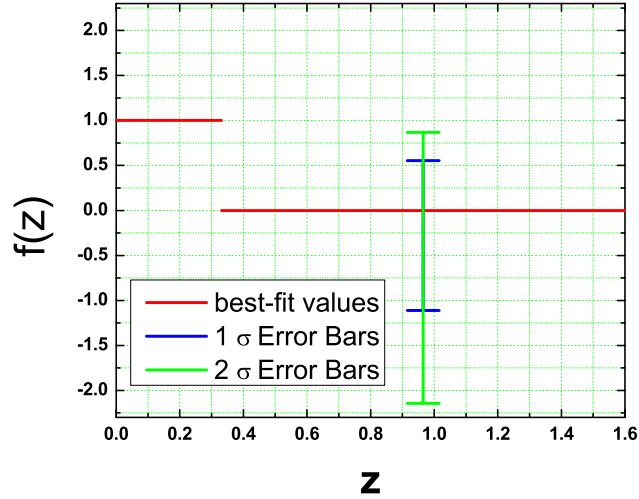


FIG. 3: Estimates of  $\rho_{\Lambda}/\rho_{\Lambda 0}$  of the  $\Lambda$ CDM2 model. Only the Constitution SNIa sample is used in the analysis. This figure shows a deviation from the  $\Lambda$ CDM over  $1\sigma$  CL.

TABLE I: Three toy models that mimic the step function

Model	Toy1	Toy2	Toy3
$f(z)$	$\frac{1+\xi^{-1}}{\xi^{-1}+\xi^{-3z}}$	$\frac{1+\xi^{-1}}{\xi^{-1}+\xi^{-sz}}$	$\frac{1}{1+e^{(z-z_0)/v}}$
$\chi_{min}^2$	457.805	457.499	456.771

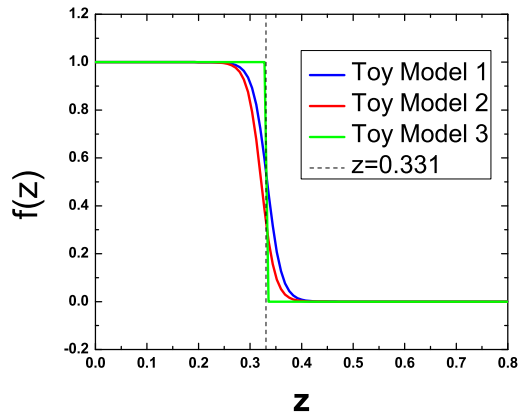


FIG. 4: The evolution of DE density  $\rho_\Lambda$  of three toy models.

parameters are  $\Omega_{m0} = 0.462$ ,  $\xi = 2.644 \times 10^{-11}$  and  $s = 3.108$ , corresponding to  $\chi^2_{min} = 457.499$ ; for toy model 3, the best-fit model parameters are  $\Omega_{m0} = 0.462$ ,  $z_0 = 0.329$ , and  $v = 4.514 \times 10^{-11}$ , corresponding to  $\chi^2_{min} = 456.771$ . Notice that the numbers of free parameters of these three toy models are less than or as same as that of CPL parameterization, so both these three models perform better than CPL parameterization in fitting the Constitution set. we also plot the evolution of  $f(z)$  of these three models in figure 4, where the best fit parameters of each model are adopted. It is seen that all these three models have a sharp decrease in  $\rho_\Lambda$  at  $z \sim 0.33$ , which is consistent with the  $\Lambda$ CDM2 model and the XCDM2 model.

As is shown in figure 5, we also take the influence of BAO and CMB data into account. Using the SNIa+BAO data, the best-fit  $\Lambda$ CDM2 model has a discontinuity point  $z_1 = 0.975$ , and its best-fit value and Corresponding  $1\sigma$  CL of the model parameters are  $\Omega_{m0} = 0.277^{+0.026}_{-0.025}$  and  $\epsilon_2 = 7.813^{+40.243}_{-6.298}$ , corresponding to  $\chi^2_{min} = 461.906$ . Using the SNIa+BAO+CMB data, the best-fit parameters of  $\Lambda$ CDM2 model has a discontinuity point  $z_1 = 0.859$ , and its best-fit value and Corresponding  $1\sigma$  CL of the model parameters are  $\Omega_{m0} = 0.283^{+0.024}_{-0.023}$  and  $\epsilon_2 = 1.677^{+0.949}_{-0.732}$ , corresponding to  $\chi^2_{min} = 463.552$ . Therefore, although the step function model in which  $\rho_\Lambda$  rapidly decreases at redshift  $z \sim 0.331$  is very powerful in fitting the SNIa data, it is not the best model to fit the combination of SNIa, BAO and CMB data. This shows the existence of the tension among different types of observational data [32]. This result is similar to the result of CPL parameterization.

For a complete comparison, using SNIa, SNIa+BAO, and SNIa+BAO+CMB data, we list  $\chi^2_{min}$ ,  $\chi^2_{min}/dof$ , and  $BIC$  for XCDM2 model and  $\Lambda$ CDM2 model in table II, table III, and table IV, respectively. It is seen that the  $\chi^2_{min}$  of  $\Lambda$ CDM2 model are very close to those of XCDM2 model. However, since the number of free parameters of  $\Lambda$ CDM2 model is one fewer than that of XCDM2 model, the  $\chi^2_{min}/dof$

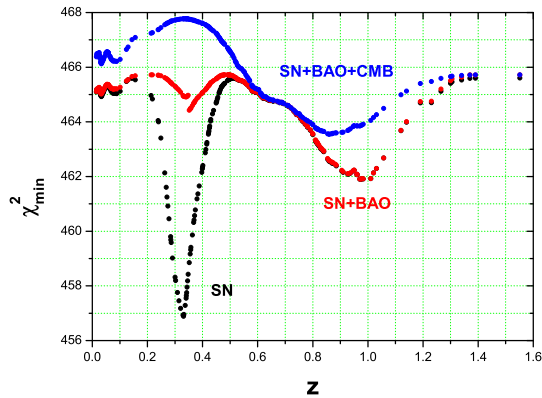


FIG. 5:  $\chi_{min}^2$  versus redshift  $z$  for  $\Lambda$ CDM2 model, where SNIa, SNIa+BAO, and SNIa+BAO+CMB data are used, respectively.

TABLE II: The  $\chi_{min}^2$  for XCDM2 model,  $\Lambda$ CDM2 model and CPL parameterization

Model	SNIa	SNIa+BAO	SNIa+BAO+CMB
XCDM2	456.574	462.500	464.775
$\Lambda$ CDM2	456.893	461.906	463.552
CPL	461.254	465.440	466.100

and  $BIC$  of  $\Lambda$ CDM2 model are smaller than those of XCDM2 model. This means the  $\Lambda$ CDM2 model performs better than the XCDM2 model in fitting the observational data. To make a further comparison, we also list the  $\chi_{min}^2$ ,  $\chi_{min}^2/dof$ , and  $BIC$  for CPL parameterization, respectively. One can see that, for SNIa, SNIa+BAO, and SNIa+BAO+CMB data, the  $\chi_{min}^2$  and  $BIC$  of  $\Lambda$ CDM2 model are 4.361, 3.534, and 2.549 smaller than those of CPL parameterization, the  $\chi_{min}^2/dof$  of  $\Lambda$ CDM2 model are 0.011, 0.009, and 0.006 smaller than those of CPL parameterization. Therefore, the  $\Lambda$ CDM2 model presents a significant improvement for the same data set obtained using the CPL ansatz.

### C. $\Lambda$ CDM3 and XCDM3 Model

Then, let us turn to the cases in which redshifts are separated into 3 bins. In table V, we list  $\chi_{min}^2$  and  $BIC$  for 3 bins piecewise constant  $w$  (XCDM3) model and 3 bins piecewise constant  $\rho_\Lambda$  ( $\Lambda$ CDM3) model. Comparing with the cases of 2 redshift bins, the reduction of  $\chi_{min}^2$  is very small, but the increase of  $BIC$  is

TABLE III: The  $\chi_{min}^2/dof$  for XCDM2 model,  $\Lambda$ CDM2 model and CPL parameterization

Model	SNIa	SNIa+BAO	SNIa+BAO+CMB
XCDM2	1.162	1.174	1.177
$\Lambda$ CDM2	1.160	1.169	1.171
CPL	1.171	1.178	1.177

TABLE IV: The  $BIC$  for XCDM2 model,  $\Lambda$ CDM2 model and CPL parameterization

Model	SNIa	SNIa+BAO	SNIa+BAO+CMB
XCDM2	480.510	486.446	488.731
$\Lambda$ CDM2	474.845	479.865	481.519
CPL	479.206	483.399	484.068

quite obvious. Again, one can see that the  $\chi_{min}^2$  of  $\Lambda$ CDM3 model are very close to those of XCDM3 model, but the  $BIC$  of  $\Lambda$ CDM3 model are much less than that of XCDM3 model. Therefore, for same number of bins, a piecewise constant  $\rho_\Lambda$  model always performs better than a piecewise constant  $w$  model. This shows the advantage of using  $\rho_\Lambda$ , instead of  $w$ , to probe the variation of DE.

We will not discuss the result of the  $\Lambda$ CDM3 and XCDM3 model explicitly. Here we only mention that the second bins of the  $\Lambda$ CDM3 and XCDM3 models also show a sharp decrease in  $\rho_\Lambda$ , as is consistent with the CPL parameterization, the  $\Lambda$ CDM2 model and the XCDM2 model. We get the minimal  $\chi_{min}^2 = 455.112$  at two discontinuity points  $z = 0.331$  and  $z = 0.975$ , and plot best-fit values and  $1\sigma$  CL of  $\rho_\Lambda/\rho_{\Lambda 0}$  for the  $\Lambda$ CDM2 model in figure 6. As is consistent with figure 1, figure 4 and figure 3, this figure also shows a visible decrease of  $\rho_\Lambda$  at  $z > 0.331$  and a deviation from the  $\Lambda$ CDM in  $1\sigma$  CL. Notice that the Error Bar of the third bin is too big to get any convincing information, the reason is that there are only 20 supernovae in this bin.

TABLE V: The  $\chi_{min}^2$  ( $BIC$ ) for XCDM3 model and  $\Lambda$ CDM3 model

Model	SNIa	SNIa+BAO	SNIa+BAO+CMB
XCDM3	455.713 (491.617)	459.598 (495.517)	462.028 (497.962)
$\Lambda$ CDM3	455.112 (485.032)	460.109 (490.041)	461.059 (491.004)

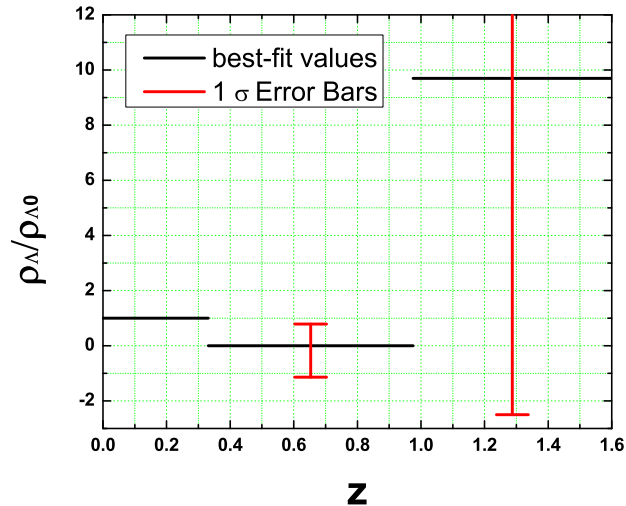


FIG. 6: Estimates of  $\rho_\Lambda/\rho_{\Lambda 0}$  of the  $\Lambda$ CDM3 model. Only the Constitution SNIa sample is used in the analysis.

## V. SUMMARY

In this work, we explore the cosmological consequences of the recently released Constitution sample of 397 SNIa. By revisiting the CPL parameterization, we find that, for fitting the Constitution set alone, the behavior of DE significantly deviate from the cosmological constant  $\Lambda$ , where  $w$  and  $\rho_\Lambda$  will rapidly decrease along with the increase of redshift  $z$ . Inspired by this clue, we separate the redshifts into different bins, and discuss the models of a constant  $w$  or a constant  $\rho_\Lambda$  in each bin, respectively. It is found that for fitting the Constitution set alone,  $w$  and  $\rho_\Lambda$  will also rapidly decrease along with the increase of  $z$ , which is consistent with the result of CPL model. Moreover, a step function model in which  $\rho_\Lambda$  rapidly decreases at redshift  $z \sim 0.331$  presents a significant improvement ( $\Delta\chi^2 = -4.361$ ) over the CPL parameterization, and performs better than other DE models. We also construct three toy models that mimic this process, and find a DE model that close to the step function model will be favored by the Constitution SNIa data. By plotting the error bars of the piecewise constant DE density of  $\Lambda$ CDM2 and  $\Lambda$ CDM3 model, we show that there is a deviation from cosmological constant  $\Lambda$  at about  $1\sigma$  confidence level; this may arise from some biasing systematic errors in the handling of SNIa data, or more interestingly from the nature of DE itself. In addition, for models with same number of redshift bins, a piecewise constant  $\rho_\Lambda$  model always performs better than a piecewise constant  $w$  model; this shows the advantage of using  $\rho_\Lambda$ , instead of  $w$ , to probe the variation of DE.

### Acknowledgements

We would like to thank Yun-Gui Gong, Bin Wang, Yi Wang, Hao Wei, Yong-Shi Wu, Yue-Liang Wu, Xin Zhang and the anonymous referee for kind help. This work is supported by the NSFC grant No.10535060/A050207, a NSFC group grant No.10821504 and Ministry of Science and Technology 973 program under grant No.2007CB815401.

- 
- [1] A.G. Riess et al., *AJ* **116**, 1009 (1998).
  - [2] S. Perlmutter et al., *ApJ* **517**, 565 (1999).
  - [3] S. Weinberg, *Rev. Mod. Phys.* **61**, 1 (1989); arXiv:astro-ph/0005265; V. Sahni and A.A. Starobinsky, *Int. J. Mod. Phys. D* **9**, 373 (2000); S.M. Carroll, *Living Rev.Rel.* **4**, 1 (2001); P.J.E. Peebles and B. Ratra, *Rev. Mod. Phys.* **75**, 559 (2003); T. Padmanabhan, *Phys. Rept.* **380**, 235 (2003); E. J. Copeland, M. Sami and S. Tsujikawa, *Int. J. Mod. Phys. D* **15**, 1753 (2006).
  - [4] B. Ratra and P.J.E. Peebles, *Phys. Rev. D* **37**, 3406 (1988); P.J.E. Peebles and B.Ratra, *ApJ* **325**, L17 (1988); C. Wetterich, *Nucl. Phys. B* **302**, 668 (1988); I. Zlatev, L. Wang and P.J. Steinhardt, *Phys. Rev. Lett.* **82**, 896 (1999).
  - [5] R.R. Caldwell, *Phys. Lett. B* **545**, 23 (2002); S.M. Carroll, M. Hoffman and M. Trodden, *Phys. Rev. D* **68**, 023509 (2003).
  - [6] C. Armendariz-Picon, T. Damour and V. Mukhanov, *Phys. Lett. B* **458**, 209 (1999) ; C. Armendariz-Picon, V. Mukhanov and P.J. Steinhardt, *Phys. Rev. D* **63**, 103510 (2001); T. Chiba, T. Okabe and M. Yamaguchi, *Phys. Rev. D* **62**, 023511 (2000).
  - [7] T. Padmanabhan, *Phys. Rev. D* **66**, 021301(R) (2002); J.S. Bagla, H.K. Jassal, and T. Padmanabhan, *Phys. Rev. D* **67**, 063504 (2003).
  - [8] M. Li, *Phys. Lett. B* **603** 1 (2004); Q.G. Huang and M. Li, *JCAP* **0408**, 013 (2004); Q.G. Huang and M. Li, *JCAP* **0503**, 001 (2005); Q.G. Huang and Y.G. Gong, *JCAP* **0408**, 006 (2004); X. Zhang and F.Q. Wu, *Phys. Rev. D* **72**, 043524 (2005); M. Li, C.S. Lin and Y. Wang, *JCAP* **0805**, 023 (2008); M. Li, X.D. Li, C.S. Lin and Y. Wang, *Commun. Theor. Phys.* **51**, 181 (2009); M. Li, X.D. Li, S. Wang and X. Zhang, arXiv:0904.0928.
  - [9] R.G. Cai, *Phys. Lett. B* **657**, 228 (2007); H. Wei and R.G. Cai, *Phys. Lett. B* **660**, 113 (2008).
  - [10] H. Wei, R.G. Cai, and D.F. Zeng, *Class. Quant. Grav.* **22**, 3189 (2005); H. Wei, and R.G. Cai, *Phys. Rev. D* **72**, 123507 (2005).
  - [11] A.Y. Kamenshchik, U. Moschella and V. Pasquier, *Phys. Lett. B* **511** 265 (2001); M.C. Bento, O. Bertolami and A.A. Sen, *Phys. Rev. D* **66** 043507 (2002); X. Zhang, F.Q. Wu and J. Zhang, *JCAP* **0601** 003 (2006).
  - [12] Y. Zhang, T.Y. Xia, and W. Zhao, *Class. Quant. Grav.* **24**, 3309 (2007); T.Y. Xia and Y. Zhang, *Phys. Lett. B* **656**, 19 (2007); S. Wang, Y. Zhang and T.Y. Xia, *JCAP* **10** 037 (2008); S. Wang and Y. Zhang, *Phys. Lett. B* **669** 201(2008).
  - [13] M. Hicken et al., arXiv:0901.4787.

- [14] M. Kowalski et al., *ApJ*. **686**, 749 (2008).
- [15] M. Hicken et al., arXiv:0901.4804.
- [16] M. Chevallier and D. Polarski, *Int. J. Mod. Phys. D* **10**, 213 (2001); E. V. Linder, *Phys. Rev. Lett.* **90**, 091301 (2003).
- [17] A. Shafieloo, V. Sahni and A.A. Starobinsky, arXiv:0903.5141.
- [18] S. Qi, T. Lu and F.Y. Wang, arXiv:0904.2832.
- [19] C.W. Chen, P. Chen and J.A. Gu, arXiv:0905.2738.
- [20] Y. Wang and K. Freese, *Phys. Lett. B* **632**, 201 (2006).
- [21] D. Huterer and G. Starkman, *Phys. Rev. Lett.* **90**, 031301 (2003); D. Huterer and A. Cooray, *Phys. Rev. D* **71**, 023506 (2005).
- [22] S. Sullivan, A. Cooray and D.E. Holz, *JCAP* **0709**, 004 (2007).
- [23] S. Qi, F.Y. Wang and T. Lu, *Astron.Astrophys* **483**, 49 (2008); S. Qi, F.Y. Wang and T. Lu, *Astron.Astrophys* **487**, 853 (2008);
- [24] Y. Wang, arXiv:0904.2218.
- [25] A.R. Liddle, *MNRAS*. **351**, L49 (2004); M. Biesiada, *JCAP*. **0702**, 003 (2007); A. Kurek and M. Szydlowski, *ApJ*. **675**, 1 (2008).
- [26] G. Schwarz, *Annals of Statistics*. **6**, 461 (1978).
- [27] S. Nesseris and L. Perivolaropoulos, *Phys. Rev. D* **72**, 123519 (2005); L. Perivolaropoulos, *Phys. Rev. D* **71**, 063503 (2005); S. Nesseris and L. Perivolaropoulos, *JCAP*. **0702**, 025 (2007).
- [28] D.J. Eisenstein et al., *ApJ*. **633**, 560 (2005).
- [29] E. Komatsu et al., *ApJS*. **180**, 3301 (2009).
- [30] J.R. Bond, G. Efstathiou and M. Tegmark, *MNRAS*. **291**, L33 (1997).
- [31] Y. Wang and P. Mukherjee, *ApJ*. **650**, 1 (2006).
- [32] H. Wei, arXiv:0906.0828.
- [33] Q.J. Zhang and Y.L. Wu, arXiv:0905.1234.